

Accepted Manuscript

Textural modification of 3D printed dark chocolate by varying internal infill structure

Sylvester Mantihal, Sangeeta Prakash, Bhesh Bhandari



PII: S0963-9969(18)30981-5

DOI: <https://doi.org/10.1016/j.foodres.2018.12.034>

Reference: FRIN 8159

To appear in: *Food Research International*

Received date: 3 December 2018

Revised date: 19 December 2018

Accepted date: 22 December 2018

Please cite this article as: Sylvester Mantihal, Sangeeta Prakash, Bhesh Bhandari , Textural modification of 3D printed dark chocolate by varying internal infill structure. Frin (2018), <https://doi.org/10.1016/j.foodres.2018.12.034>

This is a PDF file of an unedited manuscript that has been accepted for publication. As a service to our customers we are providing this early version of the manuscript. The manuscript will undergo copyediting, typesetting, and review of the resulting proof before it is published in its final form. Please note that during the production process errors may be discovered which could affect the content, and all legal disclaimers that apply to the journal pertain.

Textural modification of 3D printed dark chocolate by varying internal infill structure

Sylvester Mantihal, Sangeeta Prakash, Bhesh Bhandari* b.bhandari@uq.edu.au

School of Agriculture and Food Sciences, the University of Queensland, St Lucia QLD 4072, Australia

*Corresponding author.

Abstract

This study aimed to create an intricate internal structure of 3D printed chocolate by varying the infill construction. Three intricate infill patterns designed were star, Hilbert curve and honeycomb with infill percentage of 5%, 30%, 60% and 100%. Cadbury dark chocolate (Choc-1) and Callebaut bittersweet dark chocolate (Choc-2) powders were used by incorporating magnesium stearate (Mg-ST) and plant sterol (PS) powders as food additives. Printing parameters were set up with an extrusion temperature of 32°C, nozzle size of 0.78 mm and printing speed of 70 mm/s. The results showed that voids in printed samples of all three pattern with 5% infill density ranged from 60.8 ± 2.1 % to 72.2 ± 1.8 %. Voids in samples with 30% infill density ranged from 20.9 ± 2.1 % to 49.2 ± 3.6 % while with 60% infill density it ranged from 11.6 ± 2.3 % to 19.4 ± 4.2 %. Additionally, star and honeycomb infill pattern produced the most stable and tough structure at 60% infill as indicated by a higher normal force (N) to break the printed sample. Moreover, even at 100% infill percentage, 3D printed chocolate were found less hard (ranged from 82.2 ± 2.2 N to 92.2 ± 1.3 N) as compared to cast samples (>110 N) in the snap test. The results obtained in this study provide a useful insight in creating various internal structures of 3D printed dark chocolate with different textural characteristic and physical stability.

Keywords: 3D food printing, Infill pattern, Infill percentage, void fraction

1. Introduction

The application of 3D printing technology in food provides an excellent opportunity to create complex and innovative products. The 3D printing is a layer-by-layer deposition process in which each layer is deposited and overlap on each other to create a desired 3D shape. This technology has the potential to personalise products either in shapes and/or nutritional requirement. Currently, there are attempts made by different research groups in investigating various food materials as an edible ink for 3D food printing (3DFP) such as chocolate (Hao et al., 2010), mashed potato derived from potato flakes (Liu, Bhandari, Prakash, & Zhang, 2018), cheese (Le Tohic et al., 2018) and cereal-based product (Severini, Derossi & Azzollini, 2016). 3DFP enables the creation of a wide range of food items with variable textures, nutrients contents, taste and shapes by using a limited number of raw materials/ingredients. Texture tailored foods can be achieved by designing eccentric food structure with a computer-aided design (CAD) (Sun, Peng, Yan, Fuh, & Hong, 2015). Furthermore, multiple ingredients (varying in flavour and nutritional value) can be printed at once by using multiple cartridges; thus, it is a powerful tool in personalised nutrition applications (Liu, Zhang, Bhandari, & Wang, 2017; Jie Sun et al., 2015; Wegrzyn, Golding, & Archer, 2012; F. Yang, Zhang, & Bhandari, 2015). Cohen et al. (2009) showed the concept of creating a more extensive range of textures and tastes by mixing small group of hydrocolloids and flavours additives.

Altering structural properties in designing food to modify the textural properties such as infill structure is relatively new in 3D food printing field. Infill refers to the structure that is printed inside the 3D construct (RepRap, 2016). It is extruded in selected pattern and density and set as a parameter in the slicing software (Sli3er). Structural properties of the 3D object by varying infill structure has been investigated mostly in polymer and bio-printing. Acrylonitrile Butadiene Styrene (ABS) and Polylactic Acid (PLA) are the most common polymer used in filament printing (RepRap, 2016) and Hydrogel material (Sood, Ohdar, & Mahapatra, 2010) are commonly used in bio-printing. In Polymer printing, the tensile strength of 3D constructs was found to be dependent

on constructs' infill structure (McLouth, Severino, Adams, Patel, & Zaldivar, 2017; Sood et al., 2010). Fernandez-Vicente, Calle, Ferrandiz, and Conejero (2016) reported that honeycomb pattern was relatively tough with an increase in infill density (20%, 50% and 100%) as compared to rectilinear and line patterns. Fatimatuzaahraa, Farahaina, and Yusoff (2011) demonstrated that crisscross structure ($45^{\circ}/-45^{\circ}$) produces a higher mechanical strength (deflection, flexural and impact test) as compared to axial (0°) and transverse (90°) structures. However, cross pattern ($0^{\circ}/90^{\circ}$) showed a higher tensile strength as compared to crisscross, axial and transverse due to cross-section structure. Moreover, the tensile strength of 3D constructs printed in 0.2 mm layer thickness were stronger as compared to sample printed in 0.4 mm layer thickness (Rankouhi, Javadpour, Delfanian, & Letcher, 2016). In bio-printing field, a support structure is necessary for fabricating a stable structure for cell and tissues development (Murphy & Atala, 2014). Kang et al. (2016) reported that cell-laden hydrogel incorporated with biodegradable polymer printed in an integrated pattern could achieve higher mechanical stability as it can maintain a stable structure as compared to hydrogel printed in the un-integrated pattern. A well-developed inner structure in 3D tissues construction such as cross-link pattern was essential to maintain the mechanical properties of the constructs (Williams, Thayer, Martinez, Gatenholm, & Khademhosseini, 2018).

Very recently, there were reports on designing internal structure of 3D constructs in order to modify the textural properties of the printed foods. Liu et al. (2018) investigated the textural and structural quality of mashed potato (soft material) by modifying infill percentage (10%, 40%, 70% and 100%) with different infill patterns (rectilinear, honeycomb and Hilbert curve) and variation in shell perimeters (3, 5 and 7 shells). They reported that firmness values 25.15 g to 144.81 g and Young modulus (487.99 Pa to 43,306.50 Pa) increased and solely affected by variation in infill density between 10% and 70%. This indicates that an increase in infill percentage will increase the mechanical strength (firmness and Young modulus) of the 3D printed mashed potato. Severini, Derossi, and Azzollini (2016) reported that the addition of an inner support structure (cross and parallel) was essential to hold the 3D printed cereal-based product for

post-processing to make the constructs more stable. In this case, the infill structure was mainly designed to aid the stability of the construct.

However, in regards to edible material, there are only a few information available mainly on soft materials (Le Tohic et al., 2018; Liu et al., 2018) of the infill structure on constructs' textural properties. Textural and physical properties are essential characteristics of any edible material as they indicate the product quality. For example, a glossy appearance and snap is a common way to determine a good quality of the chocolate product (Beckett, 2008). A good snap is the ability to break apart easily and related to mechanical properties of chocolate. The snap- ability of 3D printed chocolate could be influenced by the modification textural properties by varying the infill structure in the construct. To our knowledge, there is no information regarding the modification of the textural properties of a 3D printed chocolate. Therefore, we aim to investigate the effect of internal structure on the mechanical properties of 3D printed chocolate by varying infill patterns and infill percentage. We will compare the mechanical properties of 3D printed chocolate with conventional cast chocolate samples.

2. Materials and methods

2.1.1 Materials

Two types of dark chocolates, Cadbury dark chocolate (Choc-1) and Callebaut dark chocolate button (Choc-2) purchased locally were used in this study. A commercial Cadbury chocolate was used as a control without any incorporation of flow enhancer. The composition of Cadbury dark chocolate was 53% (minimum) cocoa solids, 35% (minimum) of cocoa butter, and 0.5% lecithin. Callebaut dark chocolate button (bittersweet flavour, Lindt Piccoli) was composed of 58% (minimum) cocoa solids, 33% (minimum) cocoa butter, 5% anhydrous milk fat, 0.5% lecithin and vanilla. Both dark chocolates were ground to powders in a controlled temperature room (~ 5°C). Magnesium stearate (Mg-ST) or plant sterol (PS) was added into Choc-2 samples. 5% (w/w) of Mg-ST were added into 100g grounded Choc-2 and 3% (w/w) PS were added into 100g of grounded Choc-2. It is recognised as GRAS and was also used in the previous study

(Mantihal, Prakash, Godoi, & Bhandari, 2017). Mg-ST is an approved food additive by FDA and FSANZ and generally considered safe for consumption at an amount of 2.5g/kg body weight per day (FSANZ, 2016; Allen, 2009). Meanwhile, PS was added as a processing and nutritional aid. According to FSANZ, more than 3% of PS added to food would diminish its vital purpose as lowering LDL (FSANZ, 2016). Hence, we added approximately 3% as per the recommendation.

2.1.2 Chocolate casting procedure

Casting samples were prepared to compare the textural property of layer-by-layer deposited 3D printed chocolate with the bulk chocolate with same dimension as that of printed sample. Prior casting, chocolate formulations with and without flow enhancer were melted at around 32°C using a chocolate melting machine (ChocEdge, UK). Melted chocolate samples (with and without flow enhancer) were poured into a 3D printed cast (in house printed using Acrylonitrile Butadiene Styrene (ABS) filament, see Figure 1) covered by a thin layer of transparent plastic wrap. All samples were kept in refrigeration at around 15°C until the initiation of analysis.

2.1.3 3D-chocolate printing

3D-chocolate printing consisted of 3 steps: (1) geometry design, (2) slicing and (3) printing.

- **Geometry design:** Chocolate structures (40.0 mm diameter and 10.0 mm height) were designed using a TinkerCad online software.
- **Slicing:** The 3D design was uploaded into the Repetier-Host software (in STL file) and sliced using Slic3r to generate g-code for each model. The perimeter was set at default 3 shells approximately ~ 2.34 mm thickness considering the nozzle diameter is 0.78 mm. Three different infill structures (1) Star (2) Honeycomb and (3) Hilbert curve were chosen with a variation of infill percentage 5%, 30%, 60% and 100% for each infill pattern as shown in Figure 2. The infill structures pattern were adapted from Liu et al. (2018) for mashed potato.

- **Printing:** 3D chocolate PORIMY 1.0 (PORIMY, Kunshan, China) equipped with a rotary extrusion system used in this study is illustrated in Figure 3. Prior extrusion process, the nozzle temperature was set at 32°C for 5 min to ensure a controlled extrusion temperature is maintained. Printing speed set in the slicer software was 70 mm/s. The nozzle diameter used was 0.78mm. These printing parameters were optimized in a previous study (Mantihal et al., 2017). The printer bed temperature was maintained between 15°C and 16°C by a recirculating water system. All samples were sliced independently (specific g-code extracted for each 3D model) according to each infill pattern and infill percentage using Slic3r. In between the printing of each chocolate samples (Choc-1, Choc-2, Choc-2+ Mg-ST and Choc-2+PS), the auger extruder was dismantled and cleaned using a cleaning detergent and RO water and dried using compressed air. This was done to ensure the hygienic operation of the 3D printer. A total of n=108 samples was prepared. All printed samples were kept in refrigeration at around 15°C until the execution of quality assessment analysis.

2.2 Shape fidelity and weight measurements of 3D printed chocolate

Digital weighing balance was used to measure the weight of each printed chocolate. A digital calliper (0-150mm, CraftRight®, Bunnings, Australia) was used to measure the diameter and height of 3D printed chocolate. The measurement (diameter and height) done in three different locations on each printed samples and the average value was reported.

2.3 Textural characterisation of 3D printed chocolate

Textural properties of 3D printed chocolate were measured using a texture analyser (model TA-XT plus, Stable microsystem, UK) and operating with Exponent version 6.1.9.0 software and a TA-42 knife blade at room temperature around 23°C. The 3D printed chocolate was placed vertically on the texture analyser platform as illustrated in the Figure 4 and supported with a

custom adjustable holder to stabilise the sample on the platform. Compression mode was used to analyse the samples at 10 mm distance. A pre-test of the speed of 1.0 mm/s and the test speed of 2.0 mm/s with 5.0g trigger force was applied. To ensure a uniform measurement, all samples (regardless of infill pattern and percentage) were measured using the same method. The measurement was conducted in triplicate and data of maximum force (N) force-displacement was extracted.

2.4 Statistical analysis

Dimensional properties (weight, height and diameter), void fraction, and mechanical strength (Force –N) were presented as mean value \pm standard deviation. Minitab version 17 (statistical software) was used to analyse the significant difference of between values using One-way Analysis of variance (ANOVA) Tukey's test (where applicable). The significant difference will be determined at p -value (p) of less than 0.05.

3. Results and discussion

3.1.1 Visual appearance of 3D printed chocolate

Figure 5 illustrates, respectively, 3D-printed chocolate constructs with the variation of infill pattern (Hilbert curve, honeycomb and Star) and infill percentage (5%, 30%, 60% and 100%). As can be seen, the 3D-printed shapes with different infill structures were able to hold a layered structure. Their physical properties are discussed in the subsequent sections.

3.1.2 Dimensional evaluation of 3D printed chocolate

Physical properties such as the construct diameter, height and weight are vital to determine the precision of the 3D printer capability in constructing pre-determined chocolate design. The weight, height and diameter of 3D printed chocolate are presented in Table 1a, 1b and 1c.

As expected, the weight of the printed chocolate was influenced by the variation (increase) in infill percentage as the construct build a higher dimension as demonstrated in Figure 6 (weight of

constructs as a function of infill percentage). This is because, as the infill percentage increased, more amount of chocolate will be extruded to fill the internal structure. The relationship between infill percentage and weight of the sample appeared non-linear with lesser weight change at higher infill percentages. As can be seen in Table 1a, in general, the weight of printed constructs increased from 5 % to 100% infill percentage regardless of all chocolate samples. In most cases, chocolate samples printed in Star and Hilbert curve infill pattern were significantly different ($p < 0.05$) than that of samples printed in honeycomb infill pattern. This condition is possibly affected by the extrusion of chocolate in pattern mesostructure as each pattern was different. Fernandez-Vicente et al. (2016) also reported that the weight of polymer (acrylonitrile butadiene styrene - ABS) printed in honeycomb infill pattern and 20% infill percentage were slight higher (15g) than samples printed in Line and Rectilinear infill pattern (14g), respectively. This is indicating that although the infill percentage is the same, a slight deviation in the weight may occur due to the influence of infill pattern.

The average weight of 5% infill percentage (regardless of chocolate samples and infill pattern) ranged from 3.83 ± 0.25 g to 5.13 ± 0.45 g. For samples with 30% infill percentage, the weight ranged from 6.99 ± 0.49 g to 9.27 ± 0.45 g. For chocolate samples with 60% infill, the variation of weight was from 9.62 ± 0.38 g to 12.51 ± 0.32 g. These findings were substantiated with Liu et al. (2018) reported that an increase in infill percentage from 10% to 70%, the construct weight significantly increased from 3 g to 9 g. Similarly, in polymer printing, Fernandez-Vicente et al. (2016) also reported that as the infill percentage increase (rectilinear infill pattern) from 20% to 100%, the 3D printed object weight dramatically increase from 10.6 g to 19.0 g. This clearly indicates that variation in infill percentage (IP) influenced the constructs weight.

The height of 3D printed chocolate (regardless of infill pattern, percentage and chocolate sample) showed similar results which ranged from 10.1mm to 10.6 mm with no significant difference at ($p < 0.05$) to the pre-designed geometry as shown in Table 1b. The height of printed constructs is probably influenced by layer height (Fanli Yang, Zhang, Bhandari, & Liu, 2018). In

chocolate extrusion, the layer height was set to be equal to the nozzle diameter (0.78 mm) to achieve a well-printed construct, which means, the nozzle (Z axis) will be lifted up to 0.78 mm in every extruded layer. In this case, there are no differences in the product height, indicating similarities with the target geometry. A similar study undertaken by Fanli Yang et al. (2018) reported that by optimizing layer height according to nozzle diameter at 1.0 mm in printing lemon juice gel, a better construct that are similar to the target geometry was produced.

Table 1c shows the results of 3D printed chocolate diameter with infill percentage of 5%, 30%, 60%, 100% with various infill patterns and cast samples. The results suggest that regardless of chocolate samples, infill percentage and patterns, there is no significant difference ($p < 0.05$) in diameter between all printed chocolate samples. Also, there was no variation in diameter observed for cast chocolate as the samples are moulded in a specific dimension (10.0 mm height and 40.0 mm diameter) in bulk and no significant difference at $p < 0.05$ was observed. These results indicate that the diameter of the printed construct was found to be similar to the target geometry. As can be seen in Table 1c, a marginal discrepancy on diameter is possibly because of the influence of the weight of the product as it building a higher construct (Mantihal et al., 2017). A similar study was done in drug-loaded tablets printing, where a small variation in the construct diameter (10.55 mm to 10.67 mm) as it is printed from 10% to 100% infill percentage. This marginal difference could be due to compressed deformation of printed object influenced by gravity effect (Liu et al., 2018).

For the chocolate sample added with flow enhancer (Mg-ST and PS), the diameter, height and weight were comparable with the dimensions of the control samples (Choc-1 and Choc-2) and no significant difference ($p < 0.05$). The results show that the particulates (Mg-ST and PS) did not affect the dimensional quality of the printed chocolate. This indicates that 3D food printing possesses the capability of producing a good quality 3D chocolate product that is similar to pre-designed shape. Overall, it is demonstrated that 3D food printing is able to produce a precise and reproducible 3D printed chocolate.

3.1.3 Voids of 3D printed chocolate

Figure 6 represents the effects of infill percentages on the total weight of printed samples. As predicted, the increase in infill percentage would change the weight of the samples. This suggests that the construct weight are dependant of the infill percentage. As mentioned in section 4.6.2, the increase in weight of printed chocolate was influenced by the amount of extruded chocolate to fabricate the designated object when the infill percentage increased. This will attribute to the fact that less voids in the object as the infill percentage of the construct increased (Vancauwenberghe et al., 2017).

To determine the void fraction of 3D printed samples, the density of printed chocolate was derived from density by using volume displacement method (Liu et al., 2018). The weight of 3D printed chocolate samples and cast chocolate was obtained using a digital balance. The theoretical volume was obtained by dividing the weight by the density (1.1 g/cm^3). The void fraction of each sample was determine by the equation “*void fraction (%) = $(V_{de} - V_{th})/V_{de} \times 100$* ” adapted from Liu et al. (2018), where the V_{de} is the volume of the 3D designed geometry model (12.57cm^3), and V_{th} is the actual volume of the 3D printed chocolate samples. Void fraction (%) of all 3D printed chocolate samples Choc-1, Choc-2, Choc-2+Mg-ST and Choc-2+PS are shown in Table 2.

As can be seen in Table 2, the void fraction of 5% of 3D printed chocolate was larger ranging from $60.79 \pm 2.07 \%$ to $72.17 \pm 1.84 \%$. Larger voids in 5% infill percentage contributed by less amount of chocolate extruded to fill the internal structure as can be seen in Figure 5. Therefore, greater hollow structure is visible as compared to samples printed in 30% and 60% infill percentage (IP). As the IP increased to 30%, the voids fraction were ranging from $20.95 \pm 2.13 \%$ to $49.21 \pm 3.57 \%$. A similar trend also can be observed when the IP increase to 60%, the voids are reduced (ranging from $11.65 \pm 2.31 \%$ to $19.42 \pm 4.22 \%$), respectively. For samples printed in 100% IP, the voids are marginally ranging from $0.46 \pm 1.54 \%$ to $0.91 \pm 1.38 \%$. No voids were recorded for cast samples as the chocolate was compressed to construct the cast samples.

In most cases, the void fraction of chocolate samples printed in the same infill percentage but different infill pattern (Star, Hilbert curve and Honeycomb) are significantly different at $p < 0.05$. Also, as the infill percentage increase, the mesostructure configuration of the extruded fibre (fibre-to-fibre gap) became smaller (Rodriguez, Thomas, & Renaud, 2000). Which means, the overlapping between extruded chocolate became narrow thus reducing the voids. Another reason that could influence the construct voids is the irregularities of food material extruded during 3D printing that leads to variation in product weight (Severini, Derossi, & Azzollini, 2016). In addition, the printing path of each pattern were automated by the slicing software, and any changes are impossible to make once the parameters are set up. Therefore, a slight difference in product weight will occur thus affecting the voids. These results corroborated with Liu et al., (2018) findings reported that as the infill percentage increase from 10% to 70% the printed mashed potato voids dramatically reduced from 59.6% to 7.24%.

Besides increasing in IP, the extrudate filament can experience a swelling (increase in filament diameter) upon extrusion through the nozzle (Yousefi et al., 2018; Wang, 2012), influencing the void fraction of printed product. In thermoplastic 3D printing, the elastic behaviour of polymer led to the swelling of extrudate during deposition as reported by Nikzad, Masood, & Sbarski, (2011). Their work reported a slight increase in the extrudate filament diameter upon extrusion ranging from 1.78 mm to 1.85 mm than that of the die diameter 1.65 mm. In chocolate extrusion, 3DFP is generally optimized by default using slicing software which primarily for thermoplastic materials without any consideration in food material (Liu et al., 2018). Therefore, a marginal swelling in the chocolate filament may occur upon deposition, causing lesser void than the projected void in the target geometry (Figure 5). In addition, samples printed in HNY infill pattern show lesser void fraction (Table 2), suggesting the effect of potential swelling of extrudate filament influenced the voids. Yousefi et al., (2018) denoted that 3D-plotting condition (including the printing pathway) can affect the diameter of the extruded filament. Thus, the slight swelling of extruded chocolate marginally may affect the mesostructure, contributing to

a lesser void in HNY infill than HC and Star infill pattern. The potential swelling behaviour of food materials including chocolate during extrusion printing is one of the areas of that should be studied further.

The results suggested that printed samples added with particulates (Mg-ST and PS) did not influence the voids of the constructs. As only limited amount of Mg-ST and PS were added into the chocolate mixture 5% w/w and 3% w/w, respectively (Mantihal et al., 2017), it is observed that Mg-ST and PS did not significantly contribute to the increase in the construct weight. The linear relationship between 3D printed chocolate weight as a function void shown in Figure 7. The R^2 of 3D printed product was ($R^2 = >0.96$) indicating an excellent relationship between weight and the void fraction as the weight increase, the void fraction tends to be lower. Overall, it is worth noting that the variation in IP contributes to a different intensity of infill structure that will influence the texture (hardness) of the printed products. The hardness of construct is related to the mechanical strength of printed dark chocolate and will be discussed in the subsequent section.

3.1.4 Mechanical strength of the 3D printed dark chocolate

Dark chocolate contains high concentrations of suspended solid particles, including sugar crystals, cocoa solids and milk fat dispersed in the continuous matrix of cocoa butter (Afoakwa, 2011). The composite of relatively hard particles including flow enhancer present in dark chocolate will contribute to a higher mechanical property (Nedomova, Trnka, & Buchar, 2013). Therefore, chocolate mixture added with flow enhancer (Mg-ST and PS) possibly will exhibit higher mechanical properties. In this case, the mechanical properties were determined by force (N) that needed to break the chocolate samples.

Figure 8 represents the graph of force (N) as a function of the distance of printed chocolate in various infill percentage 5%, 30%, 60%, 100% and cast samples in different infill pattern. As can be seen in Figure 8a - e, the increase in infill percentage also increased the force required to break the printed samples. In all cases, the first series of peaks detected while the compression

blade travelled from 0 to 2.5 mm followed by other negligible values observed until reaching 5 mm of displacement. It is important to note that the initial ~ 2.5 mm were the essential fracture peaks while the second series of peak observed (from 7 to 9 mm) are the random fracture of small pieces of the chocolate. Beckett (2008) reported that a slight displacement with a steep curve of maximum force signifies a good snap quality of chocolate.

Table 3 shows the force (N) required to break samples printed in various patterns and infill percentage (5%, 30%, 60% and 100%) and also the cast samples. As can be seen in Table 3, the force required to break all printed samples (regardless of chocolate samples and infill pattern) gradually increased as the IP increased. This indicates that the hardness of chocolate is dependent with IP. At 5%_IP, the force required to break the printed samples ranged from 1.9 ± 0.1 N to 12.4 ± 0.4 N. For samples printed in 30%_IP, the force needed to break the samples ranged from 5.5 ± 0.1 N to 35.1 ± 0.2 N. As increased in IP up to 60%, the force required to break the samples also increase ranging from 8.8 ± 0.4 N to 47.4 ± 0.5 N. The differences in the force required to break the samples is because of the intensity and stability of internal structure. As mentioned earlier, the configuration of mesostructure will be more intense as the IP increases. Thus, it will contribute to a stronger construct (Rodriguez et al., 2000). These findings were substantiated with the results reported by Liu et al. (2018) who denoted that as the infill percentage increased from 10% to 70%, the hardness of mashed potato increased from 101.2 g to 423.2 g. In polymer printing, Fernandez-Vicente et al. (2016) also reported that as IP increased from 20% to 100%, the tensile strength of ABS relatively increased from 16 MPa to 37 MPa.

Regardless of infill percentage, in most cases, the printed dark chocolate samples containing flow enhancer (Mg-ST and PS) were significantly different at $p < 0.05$ than that of control samples (Choc-1 and Choc-2). Nedomova et al., (2013) reported that the tensile strength of dark chocolate increase as the cocoa solids increased from 70% to 90%. As suggested from previous study, the additional of particulates did not influence the thermal and rheology properties of chocolate (Mantihal et al., 2017). However, the presence of solids particles will influence the

chocolate matrix, contributing to the increase of mechanical strength in dark chocolate (Nedomova et al., 2013; Svanberg, Ahrné, Lorén, & Windhab, 2011). Therefore, the addition of particulates also contributed to the increase in hardness of the printed dark chocolate.

A higher force to break the samples were recorded for cast samples (> 110 N) than that of samples printed in 100% infill pattern (regardless of infill pattern). The reduced resistance to break observed for the 3D printed constructs can be explained by weakened interactions between the particles caused by the consecutive layering deposition. In contact with air, upon extrusion of a chocolate filament, a new surface is generated, to ensure high adhesion between layers (and a closer mechanical properties of a dense structure), printing speed is essential to be controlled in combination with the nozzle diameter size. A similar comparison of the cast and printed cheese was reported by Le Tohic et al. (2018). They found that the printed cheese exhibited a high degree of meltability and showed a significantly less in hardness (by up to 49%) than that of casted cheese.

Apart from the addition of particulates and IP, infill pattern also showed influence on the mechanical strength of printed chocolate. As can be seen in Table 3, overall, there was a significant difference ($p < 0.05$) of force required to break the printed samples between HC, HNY and Star infill patterns. The discrepancy of force (N) between each infill pattern is contributed by the differences in infill structure and interlayer bonding. HC infill pattern exhibited a less force required to break the samples than that of HNY and Star infill pattern from 5%_IP to 60%_IP. It is important to note that every infill pattern is different in shape and printing path (Tronvoll, Welo, & Elverum, 2018). Figure 9 exhibit HC, HNY and Star infill patterns used in this study. As can be seen in the Figure, HC infill pattern does not incorporate a criss-cross infill structure as compared to HNY and Star infill structure. Criss-cross infill structure produces a stable and stronger construct than the unintegrated pattern (Fatimatzahraa et al., 2011; McLouth et al., 2017).

In addition to that, the trajectories and interlayer bonding zones are varied between infill patterns (Fernandez-Vicente et al., 2016). HNY and star infill pattern exhibit more bonding zones

than that of HC infill pattern. As a result, HNY and Star infill pattern produced a tougher printed construct. However, in samples printed in 100% IP, most of the infill pattern exhibited almost similar to line pattern (Figure 5). Therefore, a comparable force N required to break the samples printed in 100% IP (irrespective of infill pattern) as shown in Table 3. Overall, the results indicate that 3D food printing can substantively change the textural properties of printed chocolate. Also, based on these findings, it is proposed that by modifying the infill structure (infill pattern and percentage), the sensory perception might potentially varied, as the difference would be felt when the chocolate bitten during oral consumption.

4. Conclusion

In this study, 3D auger extrusion was successfully used to fabricate a round geometry of chocolate with various infill patterns and void percentages using powdered chocolate. Shape fidelity was observed for most of the chocolate formulations tested with minimal variations in height and diameter, in comparison with the pre-set dimensions of the shape. The density and weight of the 3D constructs were controlled by the infill percentage; feature that cannot be achieved by conventional casting methods of melted chocolate. It is worth to highlighting that the chocolate shape printed with 100% infill depicted a lower resistance to break than the same formulation prepared by casting method. This was attributed to the interfacial voids formed during the deposition of layers, causing a decay in the attraction forces between the particles (or layers) during solidification. The mechanical properties of the 3D printed chocolate were also related to the type of infill patterns. Star and honeycomb patterns showed a high mechanical property due to criss-cross integrated pattern. Our findings demonstrate that 3DP is a powerful tool to control the mechanical properties of solid-chocolate. Enhanced textural attributes can be easily controlled by varying the infill pattern and percentage. Further study is being pursued investigating the detailed sensory attributes of 3D printed chocolates in regard of infill percentage.

References

- Afoakwa, E. O. (2011). *Chocolate science and technology*: John Wiley & Sons.
- Allen, L. (2009). Stearic acid. *Handbook of pharmaceutical excipients*. 6th ed. Pharmaceutical Press and American Pharmacists Association.
- Beckett, S. T. (2008). science of chocolate.
- Cohen, D. L., Lipton, J. I., Cutler, M., Coulter, D., Vesco, A., & Lipson, H. (2009). *Hydrocolloid printing: a novel platform for customized food production*. Paper presented at the Proceedings of solid freeform fabrication symposium (SFF'09).
- Fatimatuzahraa, A., Farahaina, B., & Yusoff, W. (2011). *The effect of employing different raster orientations on the mechanical properties and microstructure of Fused Deposition Modeling parts*. Paper presented at the Business, Engineering and Industrial Applications (ISBEIA), 2011 IEEE Symposium on.
- Fernandez-Vicente, M., Calle, W., Ferrandiz, S., & Conejero, A. (2016). Effect of infill parameters on tensile mechanical behavior in desktop 3D printing. *3D printing and additive manufacturing*, 3(3), 183-192.
- FSANZ. (2016). Australia New Zealand Food Standards Code - Standard 1.3.3 - Processing Aids. Retrieved from <https://www.legislation.gov.au/Details/F2009C00724>
- FSANZ. (2016). Plant Sterols. Retrieved 19/6/2017, 2017, from <http://www.foodstandards.gov.au/consumer/nutrition/plantsterol/Pages/default.aspx>
- Hao, L., Mellor, S., Seaman, O., Henderson, J., Sewell, N., & Sloan, M. (2010). Material characterisation and process development for chocolate additive layer manufacturing. *Virtual and Physical Prototyping*, 5(2), 57-64. doi: 10.1080/17452751003753212
- Kang, H.-W., Lee, S. J., Ko, I. K., Kengla, C., Yoo, J. J., & Atala, A. (2016). A 3D bioprinting system to produce human-scale tissue constructs with structural integrity. *Nature biotechnology*, 34(3), 312.
- Le Tohic, C., O'Sullivan, J. J., Drapala, K. P., Chartrin, V., Chan, T., Morrison, A. P., . . . Kelly, A. L. (2018). Effect of 3D printing on the structure and textural properties of processed cheese. *Journal of Food Engineering*, 220, 56-64.
- Liu, Z., Bhandari, B., Prakash, S., & Zhang, M. (2018). Creation of internal structure of mashed potato construct by 3D printing and its textural properties. *Food Research International*, 111, 534-543.
- Liu, Z., Zhang, M., Bhandari, B., & Wang, Y. (2017). 3D printing: Printing precision and application in food sector. *Trends in Food Science & Technology*, 69, 83-94.

- Mantihal, S., Prakash, S., Godoi, F. C., & Bhandari, B. (2017). Optimization of chocolate 3D printing by correlating thermal and flow properties with 3D structure modeling. *Innovative Food Science & Emerging Technologies*, 44(Supplement C), 21-29.
- McLouth, T. D., Severino, J. V., Adams, P. M., Patel, D. N., & Zaldivar, R. J. (2017). The impact of print orientation and raster pattern on fracture toughness in additively manufactured ABS. *Additive Manufacturing*, 18, 103-109.
- Murphy, S. V., & Atala, A. (2014). 3D bioprinting of tissues and organs. *Nature biotechnology*, 32(8), 773-785.
- Nedomova, S., Trnka, J., & Buchar, J. (2013). Tensile Strength of Dark Chocolate. *Acta Technologica Agriculturae*, 16(3), 71-73.
- Nikzad, M., Masood, S. H., & Sbarski, I. (2011). Thermo-mechanical properties of a highly filled polymeric composites for Fused Deposition Modeling. *Materials & Design*, 32(6), 3448-3456. doi:<https://doi.org/10.1016/j.matdes.2011.01.056>
- Rankouhi, B., Javadpour, S., Delfanian, F., & Letcher, T. (2016). Failure analysis and mechanical characterization of 3D printed ABS with respect to layer thickness and orientation. *Journal of Failure Analysis and Prevention*, 16(3), 467-481.
- RepRap. (2016). RepRapWiki: G-code. Retrieved 2 March, 2016, from <http://reprap.org/wiki/G-code>
- Rodriguez, J. F., Thomas, J. P., & Renaud, J. E. (2000). Characterization of the mesostructure of fused-deposition acrylonitrile-butadiene-styrene materials. *Rapid Prototyping Journal*, 6(3), 175-186.
- Severini, C., Derossi, A., & Azzollini, D. (2016a). Variables affecting the printability of foods: Preliminary tests on cereal-based products. *Innovative Food Science & Emerging Technologies*.
- Severini, C., Derossi, A., & Azzollini, D. (2016b). Variables affecting the printability of foods: Preliminary tests on cereal-based products. *Innovative Food Science & Emerging Technologies*, 38, 281-291.
- Sood, A. K., Ohdar, R., & Mahapatra, S. (2010). Parametric appraisal of mechanical property of fused deposition modelling processed parts. *Materials & Design*, 31(1), 287-295. doi: 10.1016/j.matdes.2009.06.016
- Sun, J., Peng, Z., Yan, L., Fuh, J., & Hong, G. (2015). 3D food printing—An innovative way of mass customization in food fabrication. *International Journal of Bioprinting*, 1(1), 27-38.
- Sun, J., Peng, Z., Zhou, W., Fuh, J. Y., Hong, G. S., & Chiu, A. (2015). A Review on 3D Printing for Customized Food Fabrication. *Procedia Manufacturing*, 1, 308-319.
- Svanberg, L., Ahrné, L., Lorén, N., & Windhab, E. (2011). Effect of sugar, cocoa particles and lecithin on cocoa butter crystallisation in seeded and non-seeded chocolate model systems. *Journal of Food Engineering*, 104(1), 70-80. doi: 10.1016/j.jfoodeng.2010.09.023

- Tronvoll, S. A., Welø, T., & Elverum, C. W. (2018). The effects of voids on structural properties of fused deposition modelled parts: a probabilistic approach. *The International Journal of Advanced Manufacturing Technology*, 97(9), 3607-3618. doi: 10.1007/s00170-018-2148-x
- Vancauwenberghe, V., Katalagarianakis, L., Wang, Z., Meerts, M., Hertog, M., Verboven, P., . . . Nicolaï, B. (2017). Pectin based food-ink formulations for 3-D printing of customizable porous food simulants. *Innovative Food Science & Emerging Technologies*, 42, 138-150. doi: <https://doi.org/10.1016/j.ifset.2017.06.011>
- Wang, K. (2012). Die Swell of Complex Polymeric Systems *Viscoelasticity-From Theory to Biological Applications*: InTech.
- Wegrzyn, T. F., Golding, M., & Archer, R. H. (2012). Food Layered Manufacture: A new process for constructing solid foods. *Trends in Food Science & Technology*, 27(2), 66-72.
- Williams, D., Thayer, P., Martinez, H., Gatenholm, E., & Khademhosseini, A. (2018). A perspective on the physical, mechanical and biological specifications of bioinks and the development of functional tissues in 3D bioprinting. *Bioprinting*, 9, 19-36.
- Yang, F., Zhang, M., & Bhandari, B. (2015). Recent Development in 3D Food Printing. *Critical Review Food Science & Nutrition*, 0.
- Yang, F., Zhang, M., Bhandari, B., & Liu, Y. (2018). Investigation on lemon juice gel as food material for 3D printing and optimization of printing parameters. *LWT - Food Science and Technology*, 87, 67-76.
- Yousefi, A.-M., Smucker, B., Naber, A., Wyrick, C., Shaw, C., Bennett, K., . . . Wood, K. A. (2018). Controlling the extrudate swell in melt extrusion additive manufacturing of 3D scaffolds: a designed experiment. *Journal of Biomaterials Science, Polymer Edition*, 29(3), 195-216.

Figure 1: The self-made 3D chocolate mould generated from Tinkercad software and printed using Da Vinci 2.0 dual nozzle model XYZ printer with ABS filament.

Figure 2: 3D design of round shape (40 mm diameter) with (a) Star infill (b) Honeycomb infill (c) Hilbert curve infill patterns with a variation of infill density of 5%, 30%, 60% and 100%.

Figure 3: Schematic diagram of PORIMY Kunshan 3D chocolate printer and its printing mechanism.

Figure 4: Illustration of positioning the 3D printed chocolate samples for snap properties analysis by the texture analyser (a) lateral view and (b) Anterior view.

Figure 5: Representative pictures of 3D printed chocolate samples. The letter signify chocolate formulation (a) Choc-1_control (b) Choc-2_Control (c) Choc-2+MgST and (d) Choc-2+PS. Numerical (in a row) represent the infill patterns (1) Hilbert curve (2) honeycomb (3) star. IP means Infill percentage.

Figure 6: Representative graph of 3D printed chocolate as increase infill percentage (5%, 30%, 60% and 100%) as a function of the mean value of weight (g).

Figure 7: Representative graph of the relationship between void fraction (%) and weight of 3D printed chocolate samples with infill percentage of 5%, 30% and 60% and infill patterns of Star, Hilbert curve and Honeycomb, of all chocolate samples; Cadbury dark chocolate (Choc-1), Callebaut dark chocolate (Choc-2), Callebaut dark chocolate incorporated with Magnesium stearate (Choc-2 + MgST) and Callebaut dark chocolate incorporated with Plant sterol (Choc-2 + PS).

Figure 8: Representative graph of force (N) as a function of distance (mm) of 3DP chocolate printed in various infill pattern with various infill percentage (a) 5% (b) 30% and (c) 60% (d) 100% and (e) cast sample with a pre-test speed of 1.0 mm/s and test speed 2.0 mm/s with 5.0g of trigger load of all chocolate sample (i) Choc-1 (ii) Choc-2 (iii) Choc-2+Mg-ST and (iv) Choc-2+PS. Red lines mean the maximum force (N) recorded for 3D printed samples.

Figure 9: Representative image infill pattern of (a) Hilbert curve-HC (b) honeycomb -HNY (c) Star that applied in printing chocolate.

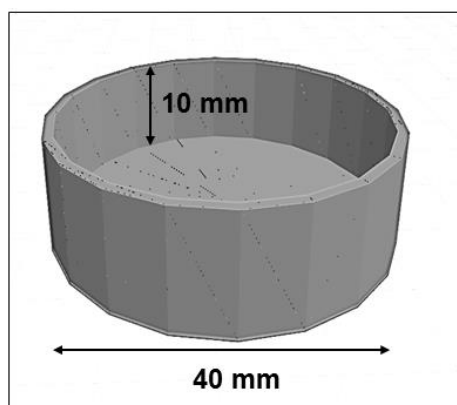


Figure 1: The self-made 3D chocolate mould generated from Tinkercad software and printed using Da Vinci 2.0 dual nozzle model XYZ printer with ABS filament.

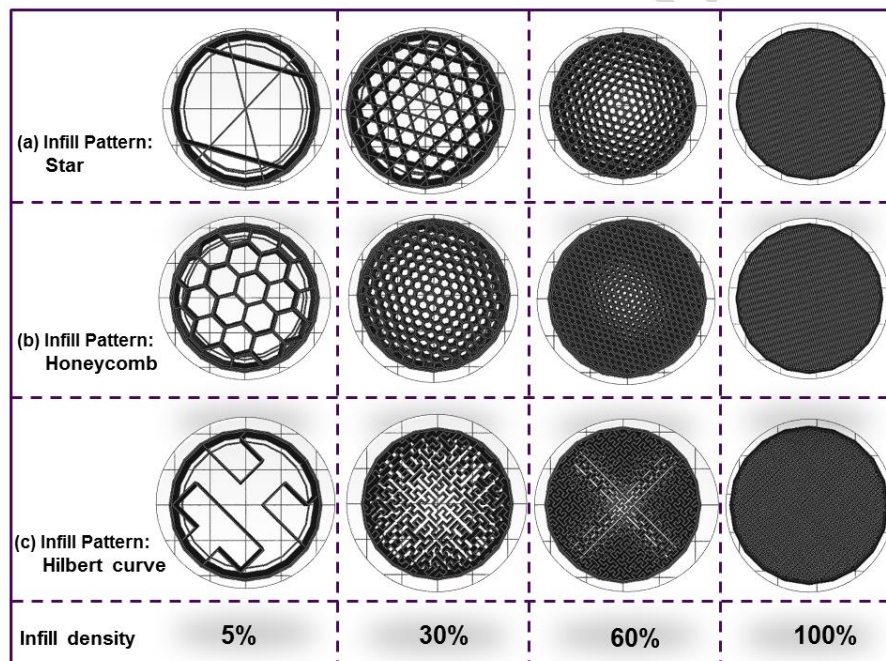


Figure 2: 3D design of round shape (40 mm diameter) with (a) Star infill (b) Honeycomb infill (c) Hilbert curve infill patterns with a variation of infill density of 5%, 30%, 60% and 100%.

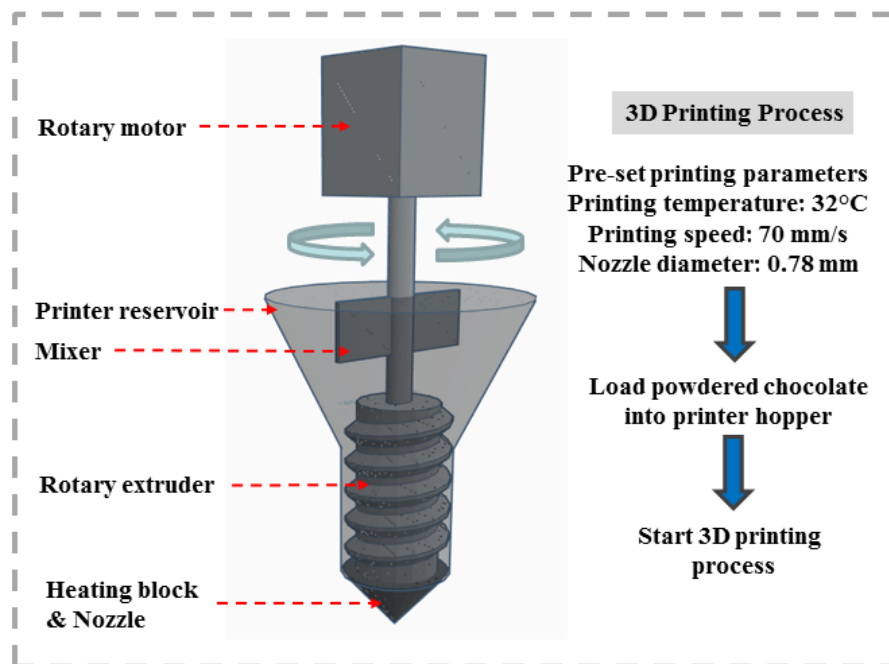


Figure 3: Schematic diagram of PORIMY Kunshan 3D chocolate printer and its printing mechanism.

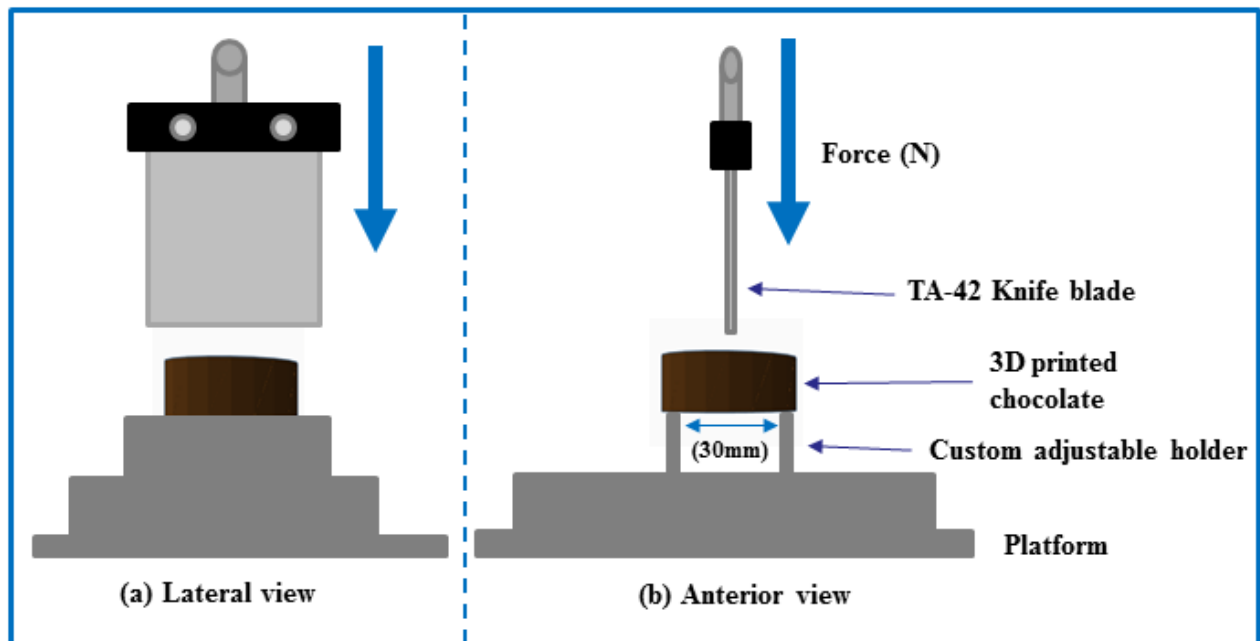


Figure 4: Illustration of positioning the 3D printed chocolate samples for snap properties analysis by the texture analyser (a) lateral view and (b) Anterior view.

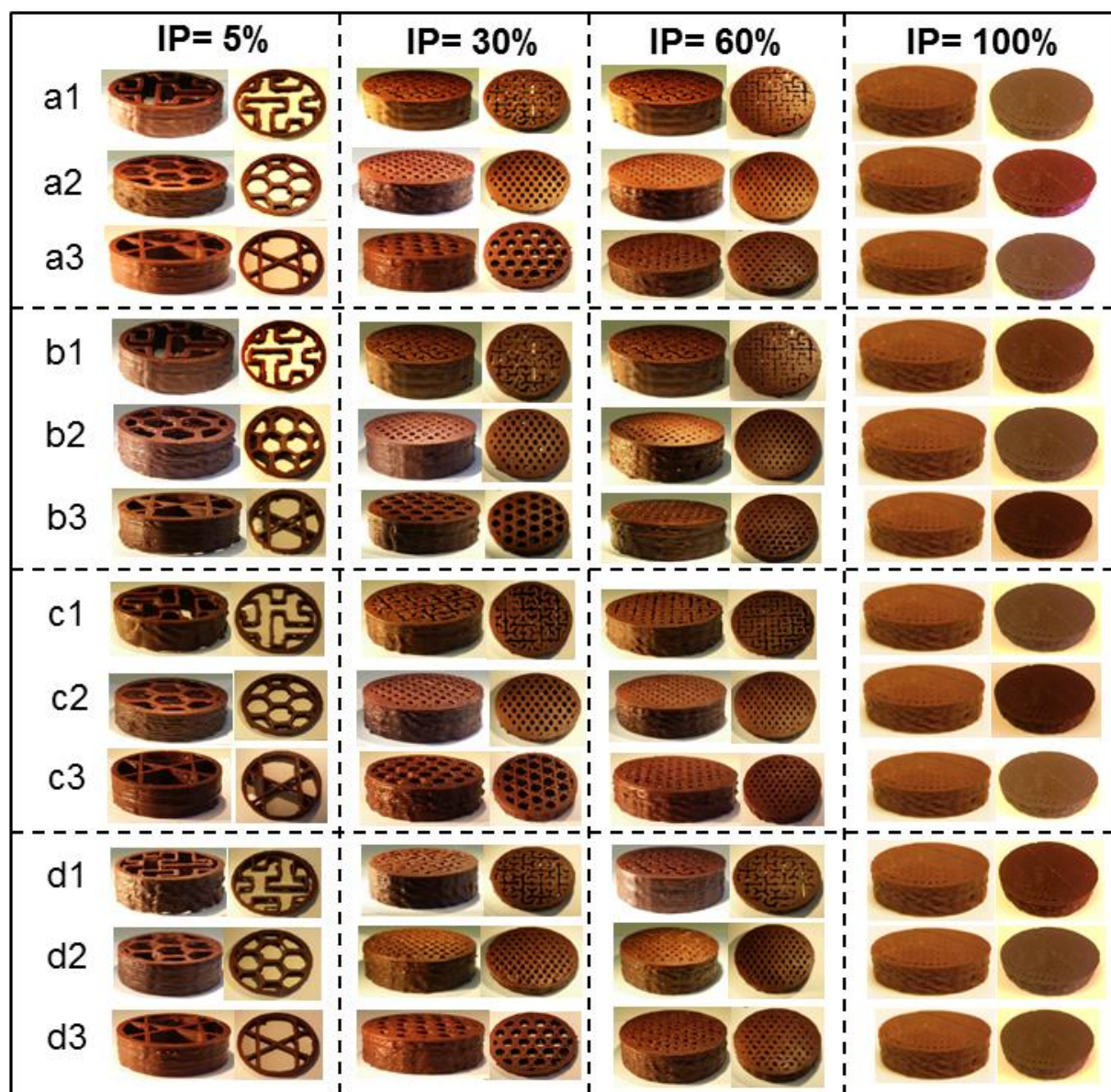


Figure 5: Representative pictures of 3D printed chocolate samples. The letter signify chocolate formulation (a) Choc-1_control (b) Choc-2_Control (c) Choc-2+MgST and (d) Choc-2+PS. Numerical (in a row) represent the infill patterns (1) Hilbert curve (2) honeycomb (3) star. IP means Infill percentage.

Table 1a: The weight of 3D printed chocolate with infill density of 5%, 30%, 60%, 100% with various infill patterns and cast. Cadbury dark chocolate (Choc-1) was without any additive while Callebaut dark chocolate (Choc-2), Callebaut dark chocolate was incorporated with Magnesium stearate (Choc-2 + Mg-ST) and Plant sterol (Choc-2 + PS).

Infill pattern	Infill percentage [%]	Weight [g]			
		Choc-1	Choc-2	Choc-2+ Mg-ST	Choc-2 + PS
Star	5	4.43 ± 0.42^a	3.78 ± 0.27^b	3.83 ± 0.25^b	5.02 ± 0.24^a
Hilbert curve	5	4.05 ± 0.40^a	4.28 ± 0.02^b	3.87 ± 0.17^b	4.42 ± 0.40^a
Honeycomb	5	4.29 ± 0.60^a	5.39 ± 0.28^a	5.13 ± 0.45^a	5.04 ± 0.21^a
Star	30	8.01 ± 0.33^a	8.36 ± 0.25^a	7.06 ± 0.34^b	8.53 ± 0.25^a
Hilbert curve	30	6.99 ± 0.49^b	8.61 ± 0.33^a	7.46 ± 0.25^b	7.49 ± 0.34^b
Honeycomb	30	8.92 ± 0.41^a	9.13 ± 0.30^b	10.88 ± 0.29^a	9.27 ± 0.45^a
Star	60	11.17 ± 0.19^a	11.68 ± 0.36^a	11.57 ± 0.26^a	11.97 ± 0.19^a
Hilbert curve	60	11.43 ± 0.61^a	11.09 ± 0.88^a	9.62 ± 0.38^b	11.57 ± 0.53^a
Honeycomb	60	11.16 ± 0.31^a	11.38 ± 0.39^a	11.58 ± 0.32^a	11.48 ± 0.32^a
All infill patterns	100	13.71 ± 0.42	13.67 ± 0.41	13.64 ± 0.35	13.69 ± 0.35
Cast sample	-	16.00 ± 0.00	16.00 ± 0.00	16.00 ± 0.00	16.00 ± 0.00

Mean value of weight (in column based on infill percentage 5%, 30% and 60%) of printed chocolate samples that does not share the same letter are significantly different at $p < 0.05$.

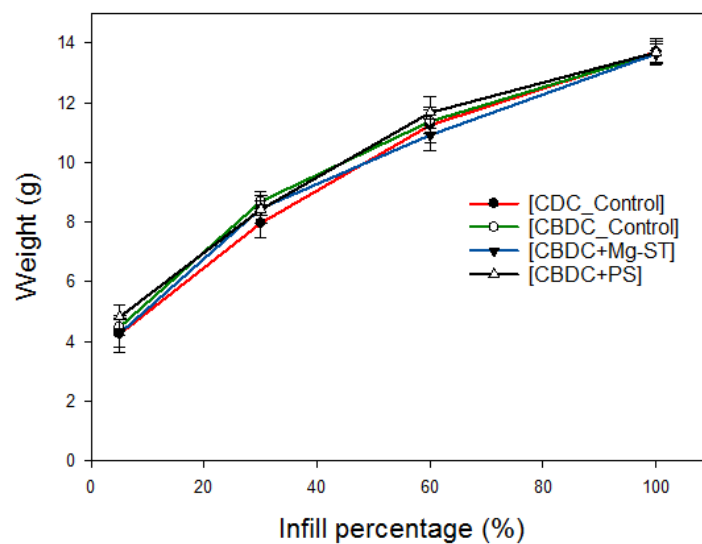


Figure 6: Representative graph of 3D printed chocolate as increase infill percentage (5%, 30%, 60% and 100%) as a function of the mean value of weight (g).

Table 1b: The height of 3D printed chocolate with infill density of 5%, 30%, 60%, 100% with various infill patterns and cast. Cadbury dark chocolate (Choc-1) was without any additive while Callebaut dark chocolate (Choc-2), Callebaut dark chocolate was incorporated with Magnesium stearate (Choc-2 + Mg-ST) and Plant sterol (Choc-2 + PS).

Infill pattern	Infill percentage [%]	Height [mm]			
		Choc-1	Choc-2	Choc-2 + Mg-ST	Choc-2 + PS
Star	5	10.2 ± 0.1 ^a	10.1 ± 0.1 ^a	10.4 ± 0.3 ^a	10.4 ± 0.5 ^a
Hilbert curve	5	10.3 ± 0.1 ^a	10.3 ± 0.1 ^a	10.2 ± 0.1 ^a	10.1 ± 0.0 ^a
Honeycomb	5	10.1 ± 0.0 ^a	10.1 ± 0.0 ^a	10.1 ± 0.1 ^a	10.4 ± 0.4 ^a
Star	30	10.2 ± 0.2 ^a	10.6 ± 0.2 ^a	10.4 ± 0.1 ^a	10.5 ± 0.3 ^a
Hilbert curve	30	10.1 ± 0.1 ^a	10.5 ± 0.1 ^a	10.5 ± 0.2 ^a	10.4 ± 0.0 ^a
Honeycomb	30	10.3 ± 0.0 ^a	10.6 ± 0.4 ^a	10.6 ± 0.2 ^a	10.6 ± 0.0 ^a
Star	60	10.3 ± 0.0 ^a	10.3 ± 0.0 ^a	10.6 ± 0.7 ^a	10.5 ± 0.1 ^a
Hilbert curve	60	10.4 ± 0.1 ^a	10.5 ± 0.1 ^a	10.5 ± 0.2 ^a	10.4 ± 0.0 ^a
Honeycomb	60	10.5 ± 0.1 ^a	10.4 ± 0.1 ^a	10.2 ± 0.1 ^a	10.1 ± 0.0 ^a
All infill patterns	100	10.3 ± 0.2 ^a	10.6 ± 0.2 ^a	10.5 ± 0.3 ^a	10.3 ± 0.3 ^a
Cast sample	-	10.0 ± 0.0 ^a	10.0 ± 0.0 ^a	10.0 ± 0.0 ^a	10.0 ± 0.0 ^a

Mean value of height (in column) that does not share the same letter are significantly different at $p < 0.05$.

Table 1c: The diameter of 3D printed chocolate with infill density of 5%, 30%, 60%, 100% with various infill patterns and cast. Cadbury dark chocolate (Choc-1) was without any additive while Callebaut dark chocolate (Choc-2), Callebaut dark chocolate was incorporated with Magnesium stearate (Choc-2 + Mg-ST) and Plant sterol (Choc-2 + PS).

Infill pattern	Infill percentage [%]	Diameter [mm]			
		Choc-1	Choc-2	Choc-2+ Mg-ST	Choc-2 + PS
Star	5	40.1 ± 0.0 ^a	40.1 ± 0.0 ^a	40.2 ± 0.2 ^a	40.2 ± 0.2 ^a
Hilbert curve	5	40.2 ± 0.0 ^a	40.2 ± 0.0 ^a	40.1 ± 0.1 ^a	40.5 ± 0.3 ^a
Honeycomb	5	40.6 ± 0.0 ^a	40.0 ± 0.0 ^a	40.1 ± 0.1 ^a	40.2 ± 0.1 ^a
Star	30	40.1 ± 0.1 ^a	40.1 ± 0.1 ^a	40.3 ± 0.2 ^a	40.1 ± 0.1 ^a
Hilbert curve	30	40.3 ± 0.1 ^a	40.3 ± 0.4 ^a	40.1 ± 0.0 ^a	40.2 ± 0.2 ^a
Honeycomb	30	40.2 ± 0.2 ^a	40.2 ± 0.5 ^a	40.1 ± 0.1 ^a	40.5 ± 0.1 ^a
Star	60	40.8 ± 0.0 ^a	40.1 ± 0.0 ^a	40.4 ± 0.0 ^a	40.2 ± 0.1 ^a
Hilbert curve	60	40.3 ± 0.1 ^a	40.7 ± 0.2 ^a	40.2 ± 0.8 ^a	40.3 ± 0.2 ^a
Honeycomb	60	40.1 ± 0.0 ^a	40.2 ± 0.0 ^a	40.2 ± 0.0 ^a	40.1 ± 0.0 ^a
All infill patterns	100	40.4 ± 0.2 ^a	40.5 ± 0.1 ^a	40.6 ± 0.1 ^a	40.3 ± 0.2 ^a
Cast sample	-	40.0 ± 0.0 ^a	40.0 ± 0.0 ^a	40.0 ± 0.0 ^a	40.0 ± 0.0 ^a

Mean value of diameter (in column) that does not share the same letter are significantly different at $p < 0.05$.

Table 2: Void fractions of 3D printed chocolate with infill density of 5%, 30%, 60%, 100% with various infill patterns and cast. Cadbury dark chocolate (Choc-1) was without any additive while Callebaut dark chocolate (Choc-2), Callebaut dark chocolate was incorporated with Magnesium stearate (Choc-2 + Mg-ST) and Plant sterol (Choc-2 + PS).

Infill pattern	Infill percentage [%]	Void Fraction [%]			
		Choc-1	Choc-2	Choc-2 + Mg-ST	Choc-2 + PS
Star	5	67.7 ± 3.1^c	72.5 ± 2.0^a	72.1 ± 1.8^a	63.5 ± 1.7^b
Hilbert curve	5	70.5 ± 2.9^a	68.8 ± 0.2^b	71.8 ± 1.2^b	67.8 ± 2.9^a
Honeycomb	5	68.7 ± 4.3^b	60.7 ± 2.1^c	62.7 ± 3.3^c	63.4 ± 1.5^b
Star	30	40.7 ± 4.3^b	39.2 ± 1.8^a	48.7 ± 2.50^a	38.0 ± 1.8^b
Hilbert curve	30	49.2 ± 3.5^a	37.3 ± 2.4^b	46.7 ± 2.1^b	45.5 ± 2.5^a
Honeycomb	30	35.1 ± 2.9^c	33.6 ± 2.2^c	20.9 ± 2.13^c	32.5 ± 3.3^c
Star	60	18.7 ± 1.3^a	15.1 ± 2.2^c	15.9 ± 1.9^b	13.0 ± 1.3^b
Hilbert curve	60	16.9 ± 3.7^b	19.4 ± 4.2^a	16.1 ± 2.7^a	16.6 ± 3.9^a
Honeycomb	60	11.6 ± 2.3^c	17.3 ± 2.6^b	15.8 ± 1.3^b	16.5 ± 2.3^a
All infill patterns	100	0.9 ± 1.3	0.6 ± 1.5	0.4 ± 1.5	0.5 ± 1.1
Cast sample	-	0	0	0	0
R ²		0.965	0.975	0.977	0.975

Mean value of void fraction (in column based on every infill percentage 5%, 30% and 60%) of printed chocolate samples that does not share the same letter are significantly different at $p < 0.05$.

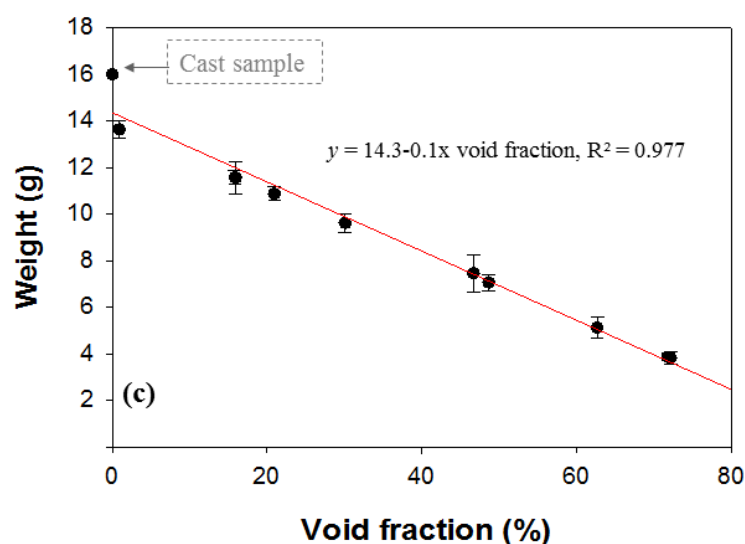


Figure 7: Representative graph of the relationship between void fraction (%) and weight of 3D printed chocolate samples with infill percentage of 5%, 30% and 60% and infill patterns of Star, Hilbert curve and Honeycomb, of all chocolate samples; Cadbury dark chocolate (Choc-1), Callebaut dark chocolate (Choc-2), Callebaut dark chocolate incorporated with Magnesium stearate (Choc-2 + MgST) and Callebaut dark chocolate incorporated with Plant sterol (Choc-2 + PS).

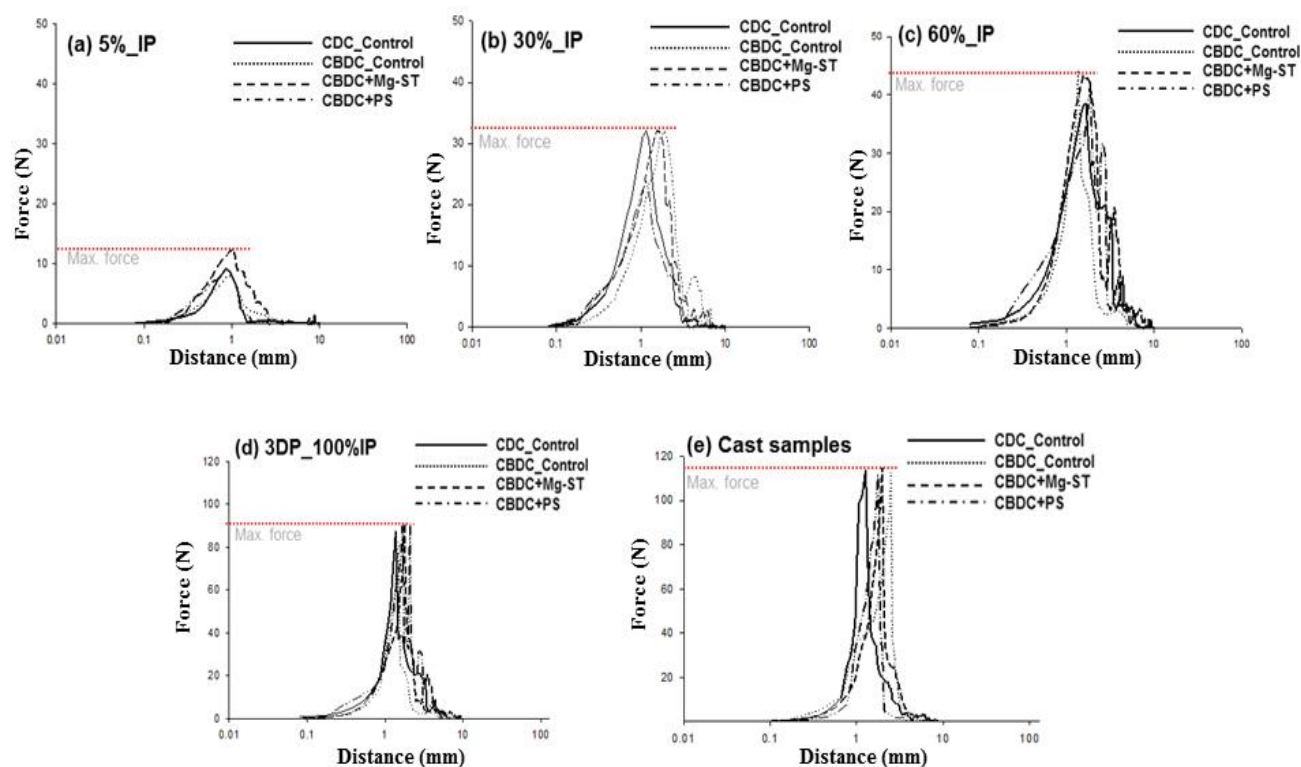


Figure 8: Representative graph of force (N) as a function of distance (mm) of 3DP chocolate printed in various infill pattern with various infill percentage (a) 5% (b) 30% and (c) 60% (d) 100% and (e) cast sample with a pre-test speed of 1.0 mm/s and test speed 2.0 mm/s with 5.0g of trigger load of all chocolate sample (i) Choc-1 (ii) Choc-2 (iii) Choc-2+Mg-ST and (iv) Choc-2+PS. Red lines mean the maximum force (N) recorded for 3D printed samples.

Table 3: Recorded force (N) to break 3D printed chocolate with different patterns and various infill percentage (5%, 30%, 60% and 100%), and cast samples.

Infill Pattern	3DP sample	Force [N]				
		[5%_IP]	[30%_IP]	[60%_IP]	[100%_IP]	[Cast]
Hilbert Curve (HC)	Choc-1(Control)	1.9 ± 0.1 ^{bF}	5.5 ± 0.1 ^{bF}	8.8 ± 0.4 ^{bF}	87.4 ± 1.6 ^{bD}	113.7 ± 4.1 ^{bA}
	Choc-2(Control)	2.1 ± 0.2 ^{bF}	5.4 ± 0.2 ^{bF}	9.4 ± 0.2 ^{bF}	82.2 ± 2.2 ^{aE}	112.5 ± 3.7 ^{aB}
	Choc-2+Mg-ST	3.5 ± 0.1 ^{aE}	5.5 ± 0.4 ^{bF}	11.1 ± 0.1 ^{aE}	90.8 ± 1.3 ^{cC}	114.5 ± 3.1 ^{bA}
	Choc-2+PS	3.2 ± 0.3 ^{aE}	6.6 ± 0.7 ^{aF}	11.7 ± 0.7 ^{aE}	92.8 ± 1.4 ^{cA}	111.2 ± 4.6 ^{aB}
Honeycomb (HNY)	Choc-1(Control)	9.2 ± 0.1 ^{bB}	31.1 ± 0.3 ^{bD}	38.2 ± 0.2 ^{bD}	88.3 ± 1.8 ^{aD}	110.3 ± 2.1 ^{bC}
	Choc-2(Control)	7.9 ± 0.5 ^{cC}	31.7 ± 0.7 ^{bD}	39.3 ± 0.3 ^{bD}	87.1 ± 1.2 ^{aD}	111.5 ± 3.2 ^{bB}
	Choc-2+Mg-ST	12.4 ± 0.4 ^{aA}	35.1 ± 0.2 ^{aA}	47.4 ± 0.5 ^{aA}	92.6 ± 1.6 ^{bA}	113.1 ± 3.1 ^{aA}
	Choc-2+PS	9.0 ± 0.3 ^{bB}	34.3 ± 1.3 ^{aB}	46.3 ± 0.9 ^{bA}	91.3 ± 1.3 ^{bB}	113.9 ± 3.7 ^{aA}
Star	Choc-1(Control)	6.7 ± 0.1 ^{bD}	28.8 ± 0.6 ^{bE}	42.8 ± 0.4 ^{bC}	87.4 ± 1.1 ^{aD}	112.1 ± 3.5 ^{aB}
	Choc-2(Control)	5.9 ± 0.4 ^{cD}	29.7 ± 0.5 ^{bE}	43.2 ± 0.1 ^{bC}	89.1 ± 1.8 ^{bC}	111.7 ± 3.7 ^{aB}
	Choc-2+Mg-ST	9.2 ± 0.2 ^{aB}	32.6 ± 0.2 ^{aC}	45.3 ± 1.4 ^{aB}	91.3 ± 1.6 ^{bB}	114.7 ± 3.1 ^{bA}
	Choc-2+PS	6.1 ± 0.2 ^{bC}	32.0 ± 0.9 ^{aC}	44.1 ± 0.3 ^{aC}	92.2 ± 1.3 ^{cA}	113.4 ± 3.6 ^{bA}

*Mean values of Force (N) that required to break the 3D printed chocolate and cast chocolate (in column based on infill percentage) that do not share a letter are significantly different at $p < 0.05$. IP means infill percentage.

*Mean values of Force (N) (in column based on infill pattern) that do not share a capital letter are significantly different at $p < 0.05$.

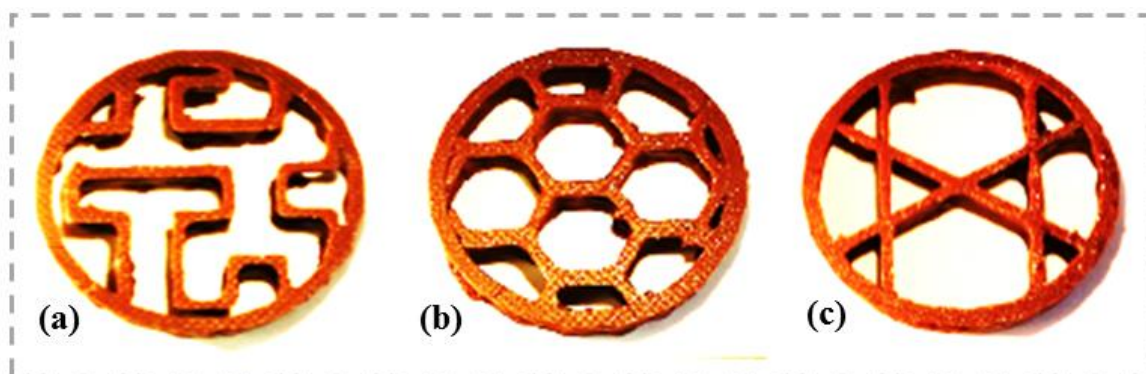


Figure 9: Representative image infill pattern of (a) Hilbert curve-HC (b) honeycomb -HNY (c) Star that applied in printing chocolate.

Highlights

- Mg-ST and PS did not affect the shape fidelity of printed chocolate.
- Void fraction of the printed chocolate was affected by increasing the infill percentage.
- Higher force (N) is required to break 3D printed samples as infill percentage increase.
- 3DFP is a powerful tool to control the mechanical properties of 3D printed food.